Final Focusing Magnetic Lenses for Light Ion Beam Fusion Reactors

E. Mogahed, L.J. Wittenberg, E. Lovell,
I.N. Sviatoslavsky, B. Choi

March 1992

UWFDM-892

Prepared for the 10th Topical Meeting on the Technology of Fusion Energy, 7–12 June 1992, Boston MA (Fus. Tech. 21 (May 1992) 1578–1582).

FUSION TECHNOLOGY INSTITUTE

UNIVERSITY OF WISCONSIN

MADISON WISCONSIN

Final Focusing Magnetic Lenses for Light Ion Beam Fusion Reactors

E. Mogahed, L.J. Wittenberg, E. Lovell, I.N. Sviatoslavsky, B. Choi

Fusion Technology Institute
University of Wisconsin
1500 Engineering Drive
Madison, WI 53706

http://fti.neep.wisc.edu

March 1992

UWFDM-892

Prepared for the 10th Topical Meeting on the Technology of Fusion Energy, 7–12 June 1992, Boston MA (Fus. Tech. 21 (May 1992) 1578–1582).

FINAL FOCUSING MAGNETIC LENSES FOR LIGHT ION BEAM FUSION REACTORS

E. Mogahed, L. J. Wittenberg, E. Lovell, I. N. Sviatoslavsky, and B. Choi
Fusion Technology Institute
University of Wisconsin-Madison
Madison, Wisconsin 53706-1687
(608) 263-1709

ABSTRACT

A magnetic lens has been designed which will focus 30 MeV Li^+ ions emitted from a diode onto a DT filled target as required in the LIBRA-LiTE fusion reactor study. Thirty such lenses are located 2.05 m from the target. Each lens is a 5 turn solenoid magnet, 0.5 m long with a bore of 0.18 m and an average B field of 1.2 tesla. Liquid Li is used as the electrical conductor and heat transfer fluid. The front end of the magnet is fabricated from porous TZM alloy with a wetted Li surface. The lifetime of the magnet in this high radiation environment is predicted to be one calendar year.

I. INTRODUCTION

The use of light ions to implode DT filled targets in commercial fusion power plants has been studied for over 10 years. This concept makes use of near term technology for the formation of high energy, pulse power generators coupled to suitable diodes from which the light ions are extracted. Several techniques have been studied for the symmetric focusing of the ion beams onto the simple direct drive targets. Initially in the LIBRA reactor study,[1] preformed ionized gas channels were suggested to transport and focus the driver ions. In the current LIBRA-LiTE reactor study[2] (a 1000 MWe fusion power plant), the 30 MeV Li^+ ions are transported ballistically to the target.[3] This choice has a profound influence on the chamber configuration because of the need to have 2 tesla final focusing magnetic lenses within 2 m from the target. The resulting neutron damage and particle flux especially on the front surface of such a magnet would be extremely severe. In addition, the reactor chamber atmosphere pressure must be low and contain no high Z vapors.

The positions of these lenses for the 24 pulse beams and 6 prepulse beams were determined by the focusing requirements of the ions and permissible radiation lifetime of the front surface of these magnets. Neutronic calculations[4] indicated that if this front surface were composed of ferritic steel its lifetime would be one calendar year at a distance of $\sim$ 2 m from the target. At this position a magnetic field strength of 0.6 tesla·m was required for each magnet with a center bore of 0.18 m. Because the electrical resistivity of any solid conductor in such a magnet would increase rapidly due to radiation damage, and a heat transfer fluid would be needed to remove the neutronic and electrical heating, liquid Li was selected as the conductor and heat transfer fluid for the magnet similar to the integrated blanket coil design by Steiner.[5] Such a magnet would be a simple one turn solenoid with a small gap running the length of the magnet, separating the positive and negative electrodes. The final lens design evolved from this concept.

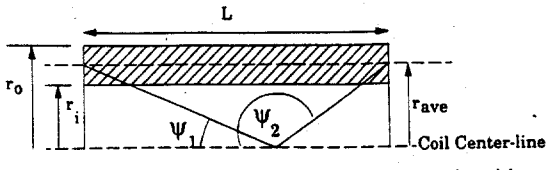

Fig. 1. Geometry of an axial section in a solenoid.

II. MAGNETIC FIELD AND CURRENT REQUIREMENTS

The requirements for the ballistic focusing have to fulfill the condition,[3]

$$LB_{ave} = 0.6 \text{ tesla} \cdot \text{m}$$

where L is the length of the magnet and B_{ave} is the average magnetic field strength. The limits imposed on the microdivergence along with the diode dimensions have legislated the design of the magnet. The magnetic field, B, due to current in the solenoid along the magnet centerline is

$$B = \mu N\, I(\cos\psi_1 - \cos\psi_2)/2L$$

where μ = magnetic permeability (vacuum); N = number of turns; I = current (A); L = magnet length (m) and the angles φ_1 and φ_2 are defined in Fig. 1. Based upon this relationship, the current and electrical power were determined for a one turn solenoid magnet whose length increased from 30 to 60 cm. As noted in Fig. 2 the required current is inversely proportional to the length of the magnet. However, increasing the length of the magnet with its center held at 2.20 m from the target decreases the distance between the magnet's face and the target which will disturb the final focus of the ions and increase the radiation to the front surface. A magnet length of 0.5 m with a magnetic field of 1.2 tesla was chosen as a compromise to fulfill all the restrictions. Figure 3 shows the variation of the magnetic field along the magnet centerline for the 50 cm magnet.

It should be noted, however, that the current of 0.647 MA for a one turn solenoid, Fig. 3, is excessive when the power dissipated in the leads to the magnet is also considered. For instance,

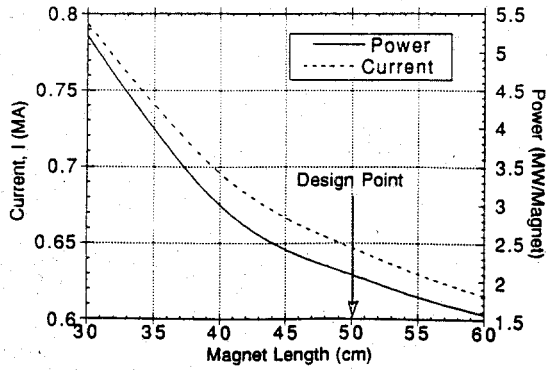

Fig. 2. Electric power dissipation and current variation with the length of the magnet for the condition: $LB_{ave} = 0.6$ tesla $\cdot$ m.

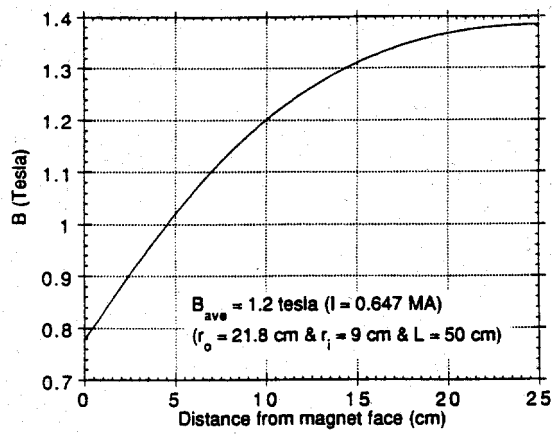

Fig. 3. Magnetic field distribution for 50 cm long and $B_{ave} = 1.2$ tesla one turn coil.

this power could be as high as 10 MW/coil or 300 MW for all 30 coils. Because this represents nearly 30% of the net electrical power produced, it was necessary to reduce this power dissipation. This power reduction was accomplished by the use of multiple turn coils. The power consumed in the coil would not change with the number of turns for the same magnetic field. However, the power consumed in the transmission lines and the magnet leads is proportional to I^2R; therefore, decreasing the value of the current is desirable.

In order to assess the value of multiple turn coils a range of coils of different lengths but with five turns was considered, Fig. 2. As noted in the figure, for coil IV, 50 cm long, the current has decreased nearly fivefold from the one turn coil design so that the power in the conductor leads should be decreased $\sim$25 times to a reasonable value of 12 MW for 30 magnets.

The five turn coil was adopted as the final design. A separately cooled front wall facing the target was utilized in order to dissipate the large surface heating. The influence of the magnetic field upon the flowing liquid metal and its subsequent effect upon the heat transfer characteristics of this coolant had to be carefully considered in the design of the magnet, as described in the following sections.

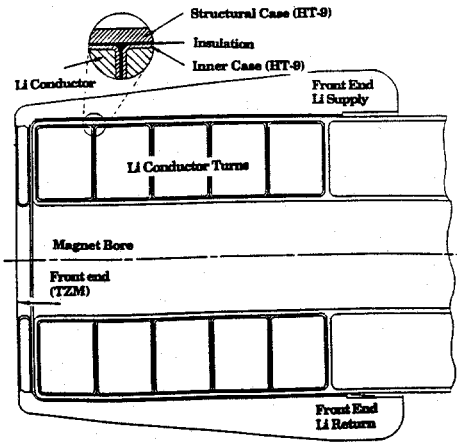

Fig. 4. Cross-section of the final focusing magnet with a sandwich construction.

III. INFLUENCE OF MAGNETIC FIELDS ON FLOWING LIQUID METALS

It has long been known that a magnetic field affects the fluid mechanics of a liquid metal[6,7] by inducing an electrical current in it perpendicular to both the magnetic field and the fluid motion. This current is the source of a retarding force that gives rise to several magnetohydrodynamic (MHD) effects. Turbulent eddies are damped by the induced magnetic force that oppose their motion and the average velocity gradient near the wall is reduced by the magnetic field. This causes the heat transfer coefficient to be substantially degraded. The flow is retarded by the ponderomotive force that acts on the bulk of the fluid causing a higher pressure drop.

The pressure increases at the axis of cylindrical liquid conductors as a result of compression by the electromagnetic pinch force due to the interaction of the electric current and its self magnetic field[7]. For homogeneous boundary conditions an electromagnetic force $f_e = J \times B$ can drive a fluid motion. The approximate estimate for the magnetic pressure generated within the fluid for a solenoid is $B^2/2\mu$. The MHD induced pressure drop, Δp, is

$$\Delta p = \sigma_w \, t_w \, u \, B^2 \, L/a$$

B	magnetic field strength (tesla)
u	average fluid velocity (m/s)
σ_w	wall electrical conductivity (1/ohm-m)
t_w	wall thickness normal to the field (m)
a	channel half width in direction of the field (m)
L	fluid path length (m)
μ	magnetic permeability of the Li.

To minimize the MHD induced pressure drop, t_w must be minimized. A sandwich construction is proposed in which the metallic layer adjacent to the lithium is as thin as feasible and is electrically insulated from a much thicker metal structural wall as shown in Fig. 4. The metallic layer facing the liquid lithium is assumed to be thin so that it essentially provides no resistance to pressure stresses, and the burden of the internal pressure is sup-

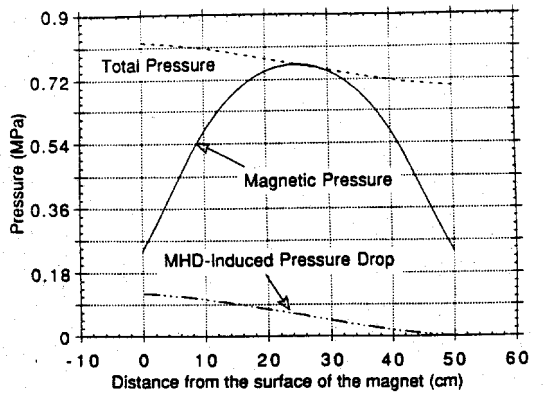

Fig. 5. Magnetic pressure and total pressure variations across the length of the magnet.

ported by a thicker structural wall outside the insulator. This design is based upon a thin inner wall of 1 mm thickness fabricated from ferritic steel, HT-9, a thin electrical insulator, $MgO{\cdot}Al_2O_3$; spinel of 0.1 mm thickness, and a thick outer HT-9 wall of 1 cm thickness determined from structural analysis. An alternative for the electrtical insulation is a polycrystalline diamond film using a chemical vapor deposition (CVD)[14] method. It is known that diamond is chemically inert and radiation-hard with thermal conductivity of 20 W/cmK, coefficient of thermal expansion of 8×10^{-7}, electrical breakdown field of 10^7 V/cm, while the operating voltage is very small compared to this value.

Figure 5 shows the magnetic pressure and the MHD induced pressure drop variation along the entire length of the magnet. The maximum pressure of 0.82 MPa is at the inlet of the liquid lithium coolant. In this study the viscous forces are small and are neglected. It is of interest to note that a high pressure must be provided to overcome the magnetic pressure hill through the first half length of the magnet; on the contrary, energy dissipators should be provided in the second half length of the magnet to avoid a strong lithium jet at the exit. The MHD induced pressure drop, Δp_{FW}, in the wall adjacent to the liquid Li is:

$$\Delta p_{FW} = 0.197 t_w \text{ (in mm) MPa.}$$

IV. THERMAL HYDRAULICS OF LAMINAR MHD CHANNEL FLOW OF A LIQUID METAL

A. Transition from Laminar to Turbulent Flow

The critical Reynolds number, Re_{cr}, increases significantly with an increase in the Hartmann number (for $Ha > 20$),[10] defined as:

Ha	Hartmann number
$(Ha)^2$	$d^2\ B^2\ \sigma/\mu$
Re	$\rho u d/\mu$ = Reynolds number
N	interaction parameter (Stuart number) = $(Ha)^2/Re$
d	channel width (meters) = $2a$
B	magnetic field strength (tesla)
u	average fluid velocity (m/s)
σ	electrical conductivity (1/ohm-m)
μ	fluid viscosity (newton-s/m^2)
ρ	fluid density (kg/m^3)

The general criterion for the transition from laminar to turbulent flow in a rectangular or circular duct can be written as $\{Re_{cr} = \text{constant} Ha\}$. It can be assumed quite reliably that the flow in any rectangular or circular duct will be laminar at $Re_{cr} < 130Ha$, while at $Re_{cr} > 215Ha$ it will be turbulent.[8] All these estimates are valid only for high Ha. In practice estimates for $Ha_R > 10$ are used, where Ha_R is the Hartmann number based on the hydraulic radius of the duct cross section.

For liquid lithium, at 400°C and $B = 2$ tesla with u (m/s) and d (m) remaining as free parameters, the results indicate Re = $1.33 \times 10^6 ud$, Ha = $1.85 \times 10^5 d$, N = $2.57 \times 10^4 d/u$. The criterion for full laminarization, $Re \leq 125Ha$, leads to $u \leq 17.4$ m/s. In practice this velocity is very large; consequently, the liquid lithium flow in the present design would be laminar most of the time.

B. Heat Transfer

The relation describing the heat transfer during steady plane parallel flow in a transverse magnetic field differs from the corresponding relation for flow without a field only by a term that accounts for ohmic heating (Joule heat generation). This term should be taken into account for liquid metals, especially if a large electrical current flows through the liquid metal or if the channel walls are conducting and the induced currents in the liquid metal are large. Although heat dissipation by viscous forces can frequently be neglected, at high Hartmann number this is not the case; the viscous and Joule dissipations are of the same order of magnitude. The magnetic field modifies the heat transfer process by changing the velocity profile. Increasing the velocity gradient near the wall results in a higher heat transfer rate. Appropriate calculations show that the heat transfer in a liquid metal (fluids with low Prandtl numbers), flowing at a moderate Hartmann number in a transverse magnetic field can increase significantly, in comparison with the case of no magnetic field. As the Hartmann number increases further, however, the rise in heat transfer rate becomes more moderate and reaches a constant value.[10] Hoffman[11] suggested that for laminar flow, the Nusselt number for fully developed flows of liquid metal between parallel plates for a constant wall heat flux can be taken as high as 12 (based on the channel hydraulic diameter).

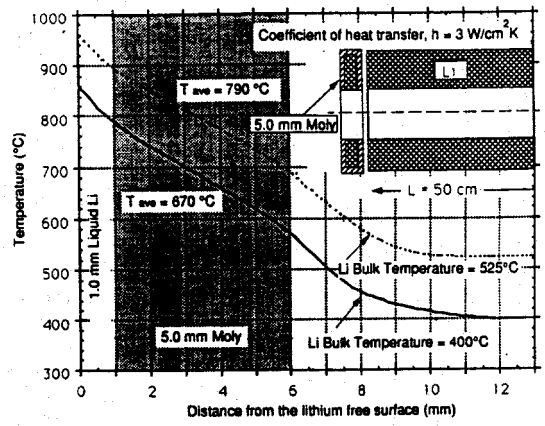

Fig. 6. The temperature distribution in the first wall, composed of the Mo alloy, TZM.

C. Thermal Hydraulics Calculations

The total thermal loads on the magnet consist of nuclear heating, ohmic heating and surface heating of the front surface facing the plasma as given in Table I. Neutronics analyses where performed utilizing a one dimensional model to calculate the distribution of the volumetric nuclear heating in the magnet.[4] Also, one dimensional hydrodynamics calculations were executed to determine the cavity performance and to account for the effects of vaporization/condensation processes on the surface heat flux.[2]

TABLE I

Thermal Hydraulic Parameters of the Coolant in the Front and Rear Section of the Magnet

Peak nuclear heating in front metal (W/cm^3)	184
Peak nuclear heating in front Li (W/cm^3)	85
Total nuclear heating/magnet (MW)	3.72
Inlet coolant temperature (°C)	275°C
Outlet temperature (°C)	525°C
Coolant temperature rise (°C)	250°C
Average coolant temperature (°C)	400°C
Coolant velocity in magnet main body (m/s)	0.83
Flow rate/main body of magnet (m^3/s)	1.06×10^{-2}
Coolant velocity in front section (m/s)	0.66
Flow rate/front section magnet (m^3/s)	1.35×10^{-3}
Total flow rate/30 magnets (m^3/s)	0.36

The total heating in the magnet is about 5.87 MW. The thermal limits of the coolant are included in Table I. Based upon these parameters the coolant velocity and flow rate were determined for the five turn magnet, Table I. The front wall has no ohmic heating because there is no current in the lithium. The total heating in the front wall including surface heating and volumetric nuclear heating is about 0.71 MW/magnet. The same temperature limits for the coolant that were applied in the coolant in the main body of the magnet were applied here too, with the results given in Table I. The total volumetric flow rate/30 magnets 0.36 m^3/s.

TABLE II

Thermal Parameters for the Front Section of the Lens

Case	First	Second
Liquid lithium temperature (°C)	400	525
Maximum temperature of TZM (°C)	780	885
Minimum temperature of TZM (°C)	580	795
Average temperature of TZM (°C)	670	790

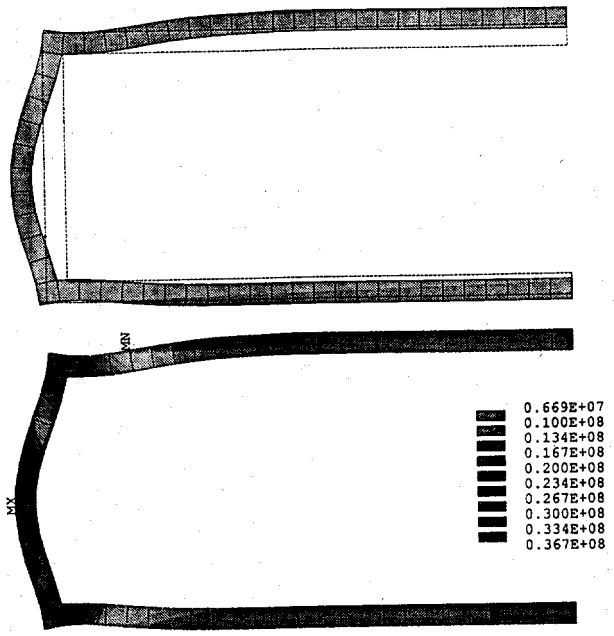

Fig. 7. Finite element deflections and stresses for quarter section (axisymmetric) of final focus magnet casing. Pressure is 1 MPa, thickness is 1 cm and material is HT-9.

A two dimensional thermal model of the first wall is used with ANSYS[12] to calculate the temperature distribution in the first wall. Two cases of the calculated temperature distribution in the front wall are shown in Fig. 6 and summarized in Table II. The first case is for the coolant at the average temperature of 400°C, while the second case is for the coolant at the maximum temperature of 525°C. The value used for the heat transfer coefficient in both cases is 3.0 W/cm^2 K, corresponding to a channel width of 16.0 mm. The Mo alloy, TZM, was chosen as the most suitable material for the first wall which can operate in this environment at this elevated temperature.

V. STRUCTURAL ANALYSIS

For the mechanical design and analysis, the casing which contains the helical magnet system can be characterized as two concentric cylindrical shells with annular end plates. No structural credit is given to the helical conduit or insulation. The primary loading is internal pressure. In the analysis, the magnitude was prescribed to be 1.0 MPa. Since stresses and deflections are linear functions of pressure, this facilitates direct scaling.

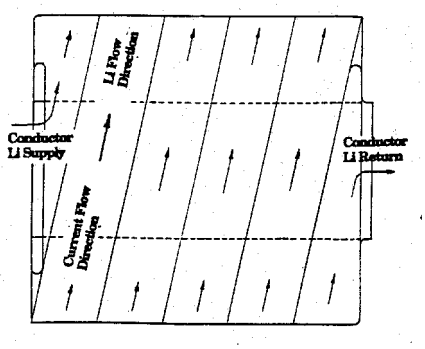

Fig. 8. Top view of the inner magnet case.

The model was analyzed both by classical methods and the finite element software ANSYS[12] with good agreement. Flexural and stretching effects were included. The particular design data presented used the fixed dimensions with the wall thickness of the two shells and end plates each equal to 1.0 cm. For HT-9 at 550°C and 150 dpa the recommended allowable stress is 115 MPa, the elastic modulus is 180 GPa and Poisson's ratio is 0.27.[13] This is the uniaxial (principal) stress with which the multidimensional equivalent stress is compared. Results for a pressure of 1 MPa are shown in Fig. 9. Maximum stress occurs near the center face of the annular end plate, 36.69 MPa, but comparable amplitudes of 34.65 MPa and 34.06 MPa develop in the larger and smaller shells, respectively, where they join the end plate. The maximum outward radial displacement of the larger shell is 23.0 μm while the inward radial displacement of the smaller shell is 5.2 μm. The maximum axial bulge in the end plate is 44.9 μm. The actual pressure is estimated to be 0.82 MPa (Fig. 5). With a scaling factor of 82%, results for maximum plate and shell stresses become 30.09 and 28.41 MPa, significantly below the given design limit. The scaled radial expansion of the outer shell is 18.9 μm while the radial contraction of the inner shell is 3.7 μm.

The thickness of individual or all components could be reduced and still have maximum stresses adequately below design limits; however, this would result in larger displacements which are not desirable. Thus a 1.0 cm thick wall is considered to be a practical specification for the magnet wall.

VI. CONCEPTUAL DESIGN OF THE FINAL FOCUS MAGNETIC LENS

In Fig. 4, a cross section of the final focus lens indicates that the five turn solenoidal channels are contained within an inner magnet case, which are electrically and hydraulically separated from the front end portion of the magnet. Removal of the outer case, Fig. 8, shows that the helical winding of the five turn coil, fabricated from rectangular tubing containing the liquid Li which is electrically insulated from the outer wall of the tubing. The outer Li and the electrical connector at the rear end of the helical magnet would be housed in the support structures for the protruding magnets. The electrical circuits for these magnets would be designed so that the exit electrodes would be nearly at ground potential.

ACKNOWLEDGEMENT

This research has been sponsored by Sandia National Laboratories and Kernforschungszentrum Karlsruhe.

REFERENCES

1. G. A. MOSES, et al., "LIBRA–A Light Ion Beam Fusion Reactor Conceptual Design," *Fusion Tech.*, **15**, 756 (1989).
2. R. R. PETERSON, et al., "LIBRA-LiTE–A Ballistic Focus Light Ion Inertial Reactor," Proc. Beams '92 Conf. 1992.
3. "Ballistic Focus Light Ion Beams for an Inertial Confinement Fusion Reactor," Proc. Beams '92 Conf. 1992.
4. M. E. SAWAN, "Neutronics Analysis for the Light Ion Beam Reactor LIBRA-LiTE," this conference.
5. D. C. STEINER, R. C. BLOCK and B. K. MALAVIYA, "The Integral-Blanket-Coil Concept Applied to the Poloidal Blanket System for a Tokamak Reactor," *Fusion Tech.*, **7**, 66 (1985).
6. R. A. GARDNER and P. S. LYKOUDIS, "Magneto-Fluid-Mechanics Pipe Flow in Transverse Magnetic Field: Part 2, Heat Transfer," *J. Fluid Mech.*, **48**, 129 (1971).
7. R. A. GARDNER, K. L. UHERKA, and P. S. LYKOUDIS, "Influence of a Transverse Magnetic Field on Forced Convection Liquid Metal Heat Transfer," *AIAA Journal 4*, **5:848** (1966).
8. H. H. BRANOVER, "Magnetohydrodynamic Flow in Ducts," John Wiley & Sons, New York, and Israel University Press, Jerusalem (1978).
9. M. PERLMUTTER and R. SIEGEL, "Heat Transfer to an Electrically Conducting Fluid Flowing in a Channel with a Transverse Magnetic Field," NASA Techn. Notes D875, 1961.
10. R. A. GARDNER, "Laminar Pipe Flow in a Transverse Magnetic Field with Heat Transfer," *Int. J. Heat Mass Transfer*, **11**, 1076-1081 (1968).
11. M. A. HOFFMAN, "Magnetic Field Effects on the Heat Transfer of Potential Fusion Reactor Coolants," Lawrence Livermore National Laboratory, UCRL-73993 (1972).
12. G. J. DeSALVO and R. W. GORMAN, "ANSYS Engineering Analysis System Users Manual," Revision 4.4, Swanson Analysis Systems, Inc., May 1989.
13. D. L. SMITH and G. D. MORGAN, "Blanket Comparison and Selection Study," Final Report, ANL/FPP-84-1 (1984) Chapter 6, p. 6.7-6.
14. L. S. PAN, D. K. KANIA, S. HAN, et al., "Electrical Transport Properties of Undoped CVD Diamond Films," *Science*, **255**, 830 (1992).